Measurement of the Birefringence of UV-Written Channel Silica Waveguides by Magnetooptic Polarization-Mode Coupling

Dietmar Johlen, Gunnar Stolze, Hagen Renner, and Ernst Brinkmeyer

***Abstract*—We report the measurement of the birefringence in integrated-optical waveguides using magnetooptical coupling between the two principal polarizations of the fundamental mode. We demonstrate this measurement technique for directly ultrviolet (UV)-written channel waveguides in silica-on-silicon and silica-on-silica. The dependence of the waveguide birefringence on the UV-writing power and UV polarization is investigated. The results are compared with the birefringence of etched waveguides in comparable material systems. An analytical formula for the form birefringence in buried channel waveguides is developed, and measured data are compared with theoretical results.**

***Index Terms*—Bragg gratings, channel waveguides, form birefringence, silica-on-silicon, ultraviolet (UV)-written waveguides, waveguide birefringence.**

I. Introduction

NTEGRATED optical waveguides in silica are used for numerous applications in optical circuits, e.g., [1]–[4]. The waveguide birefringence is one critical design parameter for the performance of these components. For etched channel waveguides in silica the birefringence has been inferred from the polarization dependence of the Bragg wavelength of ultraviolet (UV)-written gratings [5]. However, the UV-written grating itself can change the birefringence thus adulterating the measurements. It has been shown that the waveguide birefringence of etched silica-on-silicon waveguides can even be completely cancelled by UV-writing of a Bragg grating [6]. A technique for the direct measurement of the waveguide birefringence has been demonstrated for in-diffused $LiNbO_3$ channel waveguides [7] and silica fibers [8]. In this paper, we combine these two concepts and present a technique to measure the waveguide birefringence of integrated-optical silica waveguides spatially resolved by utilizing magnetooptic polarization-mode coupling. This measurement technique is demonstrated for directly UV-written channel waveguides and etched channel waveguides both in silica-on-silicon and silica-on-silica material systems. The influence of the UV exposure and UV polarization is investigated and the prospects of controlling the waveguide birefringence by UV irradiation are discussed. An analytic formula is presented for the calculation of the form birefringence of channel waveguides and applied to UV-written buried waveguides. The contributions of the form birefringence and the stress-induced birefringence resulting to the net waveguide birefringence are discussed.

Manuscript received January 25, 1999; revised October 18, 1999.

The authors are with Optik und Meßtechnik, Technische Universität Hamburg-Harburg, Hamburg, D-21073, Germany (e-mail: dietmar.johlen@icn.siemens.de).

Publisher Item Identifier S 0733-8724(00)01308-6.

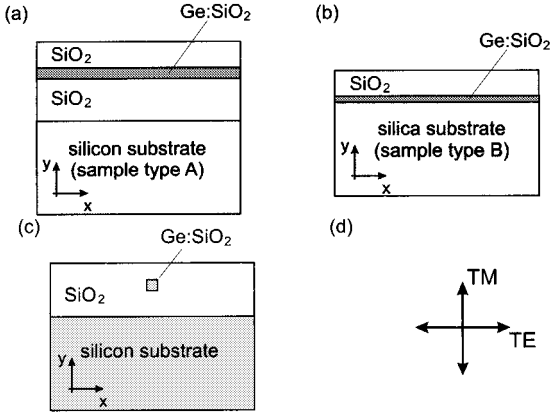

Fig. 1. (a) Endface of sample type A material. (b) Endface of sample type B material. (c) Cross section of an etched waveguide in silica-on-silicon. (d) Definitions of the polarization states TE and TM.

II. Sample Preparation

Starting point of the UV-writing of channel waveguides are commercially available (PIRI) planar waveguides on a silicon substrate for sample type A and a silica substrate for sample type B (see Fig. 1). In case of the silicon substrate there is a 20 μm buffer layer on top of the substrate. The core layer consists of 7 mol% GeO_2-doped silica resulting in a comparatively large index-difference of 0.01 ("high Δ"). For sample types A and B the core layers have thicknesses of $2a_y = 6$ μm and $2a_y = 3.5$ μm with a top cladding layer of 40 μm and 20 μm thicknesses, respectively.

A frequency-doubled Argon-Ion laser at 244 nm serves as the UV source. The UV beam is focused by a lens ($f = 10$ mm) to a spot diameter of $2a_x = 7$ μm. Channel waveguides are written using a translation stage with a step resolution of 0.5 μm at a speed of 2.5 mm/min.

Prior to the writing, the samples have been hydrogen loaded (3 mol% H_2). For both sample types a set of individual waveguides is written with varying UV-power levels P_{UV}. For sample type A the waveguides are written with a UV-writing beam polarization either directed along the waveguides (p-polarization) or perpendicular to the waveguides (s-polarization).

III. Experimental Setup for the Magneto-Optic Polarization-Mode Coupling

The birefringence is defined as

$$\delta n^{\text{eff}} = \frac{\delta\beta}{k} = \frac{\beta_{\text{TE}} - \beta_{\text{TM}}}{k} \tag{1}$$

where β_{TE} is the propagation constant of the mode mainly polarized parallel to the x coordinate, according to a pure transverse electric (TE) mode for the planar waveguide without UV treatment and β_{TM} is the propagation constant of the mode mainly polarized parallel to the y coordinate, according to a pure transverse magnetic (TM) mode for the unexposed planar waveguide as illustrated in Fig. 1(d). The wavenumber is introduced as $k = 2\pi/\lambda$, and λ is the wavelength. Effective indexes are defined as $n^{\text{eff}} = \beta/k$.

In order to measure the birefringence of integrated-optical waveguides the two polarization modes of the fundamental mode have to be coupled by some kind of localized perturbation. This has been demonstrated previously for Ti:$LiNbO_3$ waveguides by a thermooptical and an electrooptical perturbation [7] and for silica fibers with a magnetooptical perturbation [8]. When this perturbation is moved along the waveguide a beating between the two principal polarization-modes occurs, caused by the birefringence of the waveguide. The beat length l_B yields the birefringence of the channel waveguide under test

$$\delta n^{\text{eff}} = \frac{\lambda}{l_B}. \tag{2}$$

We use magnetooptic polarization-mode coupling by applying a magnetic field parallel to the waveguide as the perturbation. A spatial resolution of approximately 100 μm is achieved. The width of the magnetic field probe of 500 μm makes the alignment along the waveguide uncritical. This is an advantage for the birefringence measurement of waveguides with bends such as in directional couplers.

The experimental setup for the beat-length measurement is shown in Fig. 2. Light of a distributed feedback (DFB)-laser at $\lambda = 1549$ nm is launched in either TE or TM polarization into the waveguide under test. The magnetic field rotates the plane of polarization of the propagating mode slightly according to the Faraday effect and a small portion of light power is coupled into the orthogonal polarization. A phase difference ϕ between the waves of the two principal polarizations is accumulated due to the birefringence beginning at the perturbation up to the end of the waveguide

$$\phi(z) = \int_z^L [\beta_{\text{TE}}(z') - \beta_{\text{TM}}(z')]\, dz' \tag{3}$$

where z is the position of the perturbation and L represents the total waveguide length. The beat signal $p_1(z)$ is generated by an interference of the two principal polarization modes by an analyzer rotated by 45°. The magnetic field is modulated in order to enable synchronous detection of the beat signal.

The accuracy of the measurement is further increased by the use of an electrooptic phase modulator (EOM) in front of the analyzer acting as a $\lambda/4$ wave plate. This gives an additional beat signal, $p_2(z)$, phase-shifted by $\pi/2$. With this additional beat signal a very precise detection of the phase difference is possible [9]. A phase measurement accuracy of 6.9×10^{-3} rad over 1 cm corresponds to a resolution of the birefringence δn^{eff} better than 2×10^{-7}.

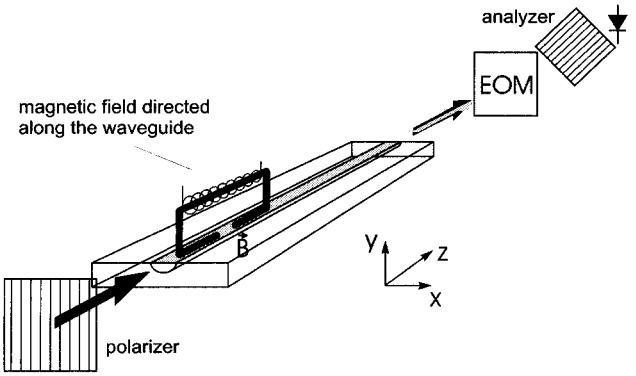

Fig. 2. Magnetic probe is scanned along a waveguide for measuring the beat-length of the two principal polarizations of the fundamental mode.

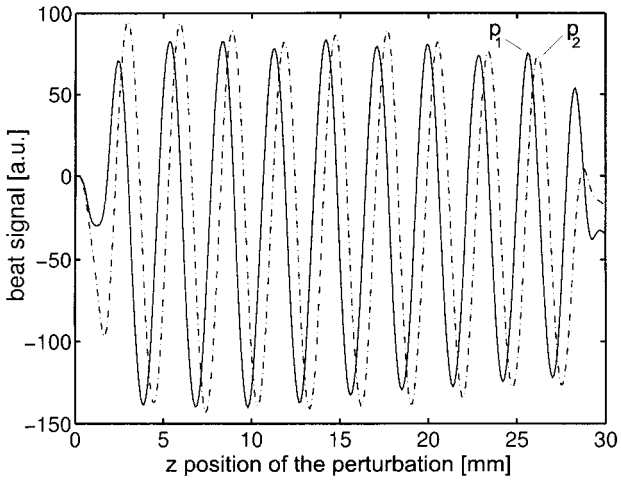

Fig. 3. Beat length measurement for a UV-written waveguide in silica-on-silicon (sample type A).

In Fig. 3 the beat signal $p_1(z)$ and the $\pi/2$ shifted signal $p_2(z)$ for a waveguide written with $P_{\text{UV}} = 20$ mW and UV-polarization perpendicular to the waveguide is shown. From the two beat signals $p_1(z)$ and $p_2(z)$ the phase difference is calculated as $\phi(z) = \arctan[p_2(z)/p_1(z)]$ and the result is displayed in Fig. 4. The slope is proportional to the birefringence (see (4))

$$\delta n^{\text{eff}} = n_{\text{TE}}^{\text{eff}} - n_{\text{TM}}^{\text{eff}} = \frac{\lambda}{l_B} = \frac{\lambda}{2\pi}\left(-\frac{d\phi(z)}{dz}\right). \tag{4}$$

From (4), we conclude a birefringence of $\delta n^{\text{eff}} = -5.51 \times 10^{-4} \pm 5 \times 10^{-6}$ for a channel waveguide written with 20 mW UV power in s-polarization in silica-on-silicon.

The relation between the sign of the birefringence and the sign of the slope of the phase $\phi(z)$ is found by measuring a waveguide for which the waveguide birefringence is known. For this experiment a grating is written simultaneously with the channel waveguide through a phase mask in silica-on-silica. The two polarization resolved transmission spectra are displayed in Fig. 5.

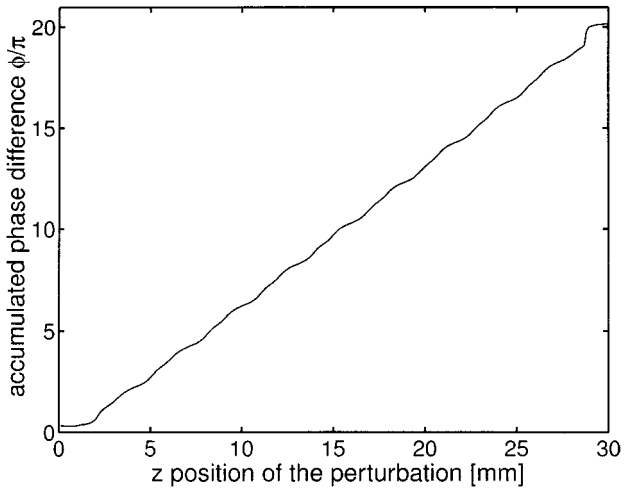

Fig. 4. Phase difference ϕ between the two principal polarizations accumulated from the probe position z up to the end of the waveguide due to birefringence [see (3)] for a UV-written waveguide in a silica-on-silicon material system (sample type A).

The difference in the Bragg wavelengths is $\Delta\lambda_B = \lambda_{B,\mathrm{TE}} - \lambda_{B,\mathrm{TM}} = 0.48$ nm, resulting in a birefringence [5] of $\delta n^{\mathrm{eff}} = 2.0 \times 10^{-4}$. The beat-length measurement yields a negative slope of $\phi(z)$ for this waveguide with positive birefringence. Thus, positive slope means $\delta n^{\mathrm{eff}} = n^{\mathrm{eff}}_{\mathrm{TE}} - n^{\mathrm{eff}}_{\mathrm{TM}} < 0$, and vice versa. The birefringence measured by the Bragg wavelength technique is in good agreement with the result $\delta n^{\mathrm{eff}} = 2.13 \times 10^{-4}$ obtained from the beat-length measurement for this waveguide. It has to be stated that the beat-length measurement is much more accurate compared to the measurement derived from the optical spectrum analyzer with a spectral resolution of 0.2 nm.

No change in birefringence is observed in a UV-written waveguide which hosts a Bragg grating at the transition "waveguide section with grating"/"waveguide section without grating." In this case, the waveguide and the Bragg grating are simultaneously written through a phase mask. Thus, only the UV exposure is of importance not the fine structure of the UV-induced index change. Note that the spatial resolution (100 μm) of the measurement cannot resolve the grating fringes in the submicron range.

IV. Experimental Results

A. Sample Type A

For sample type A two sets of waveguides have been written with UV-laser powers P_{UV} ranging from 10 mW to 100 mW in steps of 10 mW in s- and p-polarization of the writing beam. The result of the beat-length measurement is displayed in Fig. 6. In addition to the UV-written waveguides the birefringence of the planar waveguide has also been measured and is displayed in Fig. 6 at $P_{\mathrm{UV}} = 0$. For both UV polarizations a decrease of the waveguide birefringence with the UV-fluence can be observed by more than a factor of 2 compared to the birefringence of the planar waveguide. In waveguides written with even higher UV-powers the birefringence is not further reduced.

Fig.6 indicates a weak dependence of the waveguide birefringence on the polarization of the writing beam. For higher

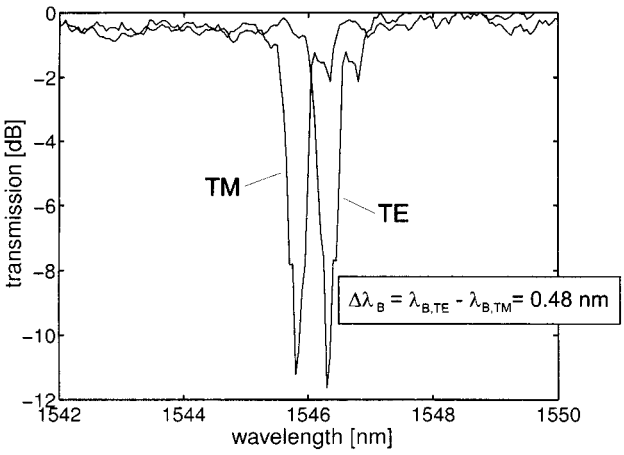

Fig. 5. Polarization resolved spectra of a UV-written Bragg grating in silica-on-silica (sample type B).

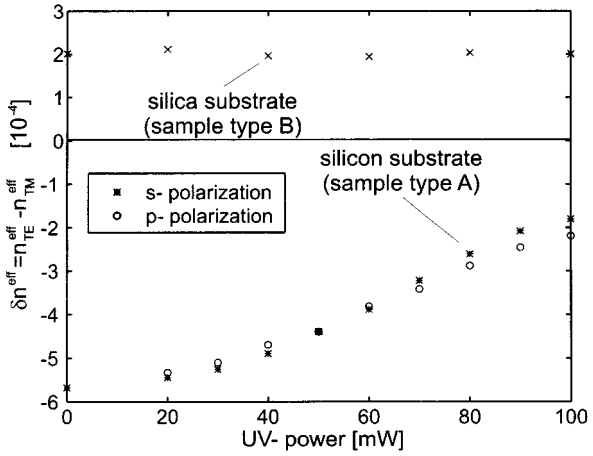

Fig. 6. Dependence of the birefringence of UV-written waveguides on the UV-writing power for silica-on-silicon and silica-on-silica substrates.

writing powers, in excess of 50 mW, the irradiation with UV light of s-polarization has more effect on changing the birefringence, whereas it has less effect at lower writing powers (see Fig. 6). It cannot be decisively determined here if this behavior for lower writing powers is significant. Due to the realignment of the setup in order to change the UV writing beam polarization a small experimental error might be imposed on the UV writing power. This can lead to a writing power offset between the two groups of waveguides. For example, an offset of approximately $+5$ mW for the power of waveguides written in s-polarization would be sufficient here to have always more effect for s-polarization on the change of birefringence than for p-polarization of the writing beam. Please note that for low writing powers the birefringence of both groups of waveguides has to converge to the birefringence of the planar waveguide.

The measured waveguide birefringence consists of stress birefringence and form birefringence. By considering the different thermal expansion coefficients of silica and silicon the stress-induced birefringence is calculated to be about $\delta n = -6 \times 10^{-4}$. This is in good agreement with the birefringence of the planar waveguide in sample type A. The calculation of the form birefringence $\delta n^{\mathrm{eff}}_F$ [see Fig. 9(a) below] shows that the planar waveguide has a positive form birefringence 25

times smaller than the measured total waveguide birefringence. The form birefringence of the UV-written waveguides with a channel width of about $2a_x = 8$ μm is nearly constant [see Fig. 9(a)] up to a UV-induced index $\Delta n_{\mathrm{UV}} = 0.012$. Thus, the form birefringence can be neglected for waveguides in sample type A. The UV-writing power $P_{\mathrm{UV}} = 100$ mW corresponds to a UV-induced index change Δn_{UV} of 0.008 measured by the refractive-near-field method. According to these results the UV writing leads to a net stress relieve or change in the stress profile expressed in a reduction of the waveguide birefringence. This does not explain why the birefringence is not reduced further down to the size of the form birefringence.

It is instructive to compare the results for UV-written buried waveguides with those of buried waveguides fabricated by etching in a material system comparable with sample type A [see Fig. 1(c)]. The index profile of these etched channel waveguides is nominally square (6 μm by 6 μm). For such waveguides no form birefringence occurs. The birefringence is measured to be about -5×10^{-4} and corresponds to the birefringence observed in the planar waveguide or UV-written waveguides with low UV-power (Fig. 6) for sample type A. This birefringence is also reduced by UV exposure to typical values of $\delta n^{\mathrm{eff}} = -2 \times 10^{-4}$ for a UV writing power $P_{\mathrm{UV}} = 100$ mW.

The waveguide birefringence reported in [3], [5], [6] for material systems comparable to sample type A is of opposite sign compared to the results presented in this paper. This might be explained by a different dopant composition of the glass layers which affects the stress induced birefringence of the waveguides.

B. Sample Type B

For sample type B a set of waveguides has been written with UV-powers ranging from 20 mW to 100 mW in steps of 20 mW without UV beam polarization control. The waveguide birefringence is almost independent of the UV-writing power and is equal to the birefringence measured for the planar waveguide (see Fig. 6). Compared to sample type A ($\delta n^{\mathrm{eff}} = n^{\mathrm{eff}}_{\mathrm{TE}} - n^{\mathrm{eff}}_{\mathrm{TM}} < 0$) the waveguide birefringence is found to have opposite sign for sample type B ($\delta n^{\mathrm{eff}} = n^{\mathrm{eff}}_{\mathrm{TE}} - n^{\mathrm{eff}}_{\mathrm{TM}} > 0$).

The form birefringence of the planar waveguide for sample type B has been calculated in Fig. 9(b). This does not fully account for the observed birefringence, and in consequence, also a stress-induced birefringence is present although material system B is nominally silica-on-silica neglecting the germanium doped core layer of the planar waveguide. This is comparable to elliptical fibers where the stress-induced birefringence can be of the order of $\delta n^{\mathrm{eff}} = 10^{-4}$ [10]. Regarding Fig. 9(b) the form birefringence increases for stronger waveguides. However, the total waveguide birefringence is unchanged (see Fig. 6). This suggests that similarly to sample type A a reduction of the stress-induced birefringence occurs. By comparing the results of Figs. 6 and 9 the stress-induced birefringence is reduced by 0.6×10^{-4}. This corresponds to 38 % reduction in stress-induced birefringence due to the UV illumination. This reduction is compensated for this material system possibly by an increase in form birefringence of the UV-written channel waveguides and no net birefringence reduction is observed in contrast to material system A.

Nearly polarization independent gratings fabricated in a silica-on-silica material system from PIRI in so-called "low Δ" samples have been reported [11]. In our case we use "high Δ" samples from PIRI and the higher germanium concentration can be responsible for the results observed in our experiments.

C. Further Discussion

The dependence of the birefringence in Bragg gratings on the UV-writing polarization has been investigated for fibers [13]. The birefringence of a fiber Bragg grating is reported there to be $|\delta n_s^{\mathrm{eff}}| \approx 5 \times 10^{-5}$ for s-polarization and $|\delta n_p^{\mathrm{eff}}| \approx 0.5 \times 10^{-5}$ for p-polarization. The sign of the birefringence was not determined in that experiment. We observe a similar polarization dependence of the birefringence for the planar sample type A if the sign of the birefringence in [13] is assumed to be positive ($n^{\mathrm{eff}}_{\mathrm{TE}} > n^{\mathrm{eff}}_{\mathrm{TM}}$) as observed in our experiments with fibers. The difference in the UV-induced birefringence in [13] for the two writing beam polarizations is then given for fibers by $\delta n_s^{\mathrm{eff}} - \delta n_p^{\mathrm{eff}} = 4.5 \times 10^{-5}$. We have analyzed the fiber birefringence by a fiber Fabry–Perot interferometer consisting of two UV-written Bragg gratings [12]. The polarization-dependent shift of the resonances of the Fabry-Perot interferometer yields the UV-induced birefringence with a typical value of $\delta n^{\mathrm{eff}} = 5 \times 10^{-5}$. The fiber was cleaved directly behind the gratings and TE and TM polarization is understood as polarization perpendicular and parallel to the direction of the UV writing beam, respectively. The reduction of birefringence for a waveguide written with $P_{\mathrm{UV}} = 100$ mW for s-polarization is larger by 4×10^{-5} than for p-polarization yielding a polarization-dependent difference of $\delta n_s^{\mathrm{eff}} - \delta n_p^{\mathrm{eff}} = 4 \times 10^{-5}$ (see Fig. 6). This suggests the presence of a small positive polarization-dependent UV-induced birefringence which is larger for s-polarization and thus reduces a negative birefringence more strongly.

V. Calculation of the Form Birefringence of Channel Waveguides

In order to analyze the form birefringence of the UV-written channel waveguides we apply Marcatili's method [14]. Since the latter gives reliable results for the form birefringence up to first order in the small refractive-index difference [15], we use a perturbation method in this small refractive-index difference for calculating the birefringence in the planar waveguides involved. We obtain an explicit analytical formula for the form birefringence in weakly guiding rectangular channel waveguides.

The refractive-index profile of our UV-written channel waveguides can be modeled in cartesian coordinates (x, y) [see Fig. 7(a)]

$$n^2(x,y) = \begin{cases} n^2_{\mathrm{UV}} & \text{for } |x| < a_x, \quad |y| < a_y, \quad \text{(UV-written core)} \\ n_f^2 & \text{for } |x| > a_x, \quad |y| < a_y, \quad \text{(film)} \\ n_s^2 & \text{for } |x| > a_x, \quad |y| > a_y, \quad \text{(substrate)} \end{cases} \tag{5}$$

where n_s and n_f are the refractive indexes of the silica substrate and of the GeO_2 doped planar film waveguide, respec-

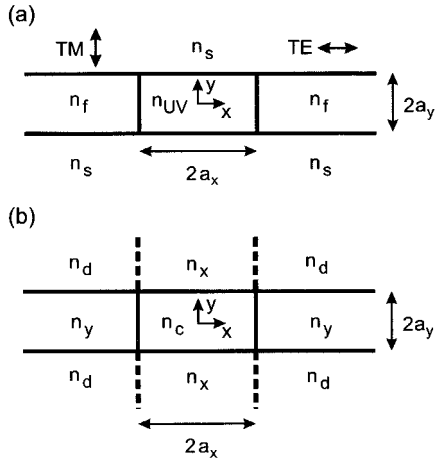

Fig. 7. (a) Refractive-index distribution of a channel waveguide fabricated by direct UV-laser beam writing in a germanosilicate film. (b) Equivalent rectangular waveguide profile composed of two planar step-index waveguide profiles. For the present analysis of UV written waveguides $n_c = n_{\rm UV} = n_f + \Delta n_{\rm UV}, n_x = n_s, n_y = n_f, n_d = (n_s^2 + n_f^2 - n_{\rm UV}^2)^{1/2}$.

tively. The refractive-index in the core of the channel waveguide is $n_{\rm UV} = n_f + \Delta n_{\rm UV}$, where $\Delta n_{\rm UV}$ represents the UV-induced increase of the refractive-index in the photosensitive germanosilicate film. According to Marcatili's analysis [14] we can approximate the profile by the superposition of two planar waveguide profiles

$$n^2(x,y) = n_d^2 + \left(n_c^2 - n_x^2\right) S\left(\frac{y}{a_y}\right) + \left(n_c^2 - n_y^2\right) S\left(\frac{x}{a_x}\right) \tag{6}$$

as shown in Fig. 7(b). Here

$$S(t) = \begin{cases} 1 & \text{for } |t| < 1 \\ 0 & \text{for } |t| > 1 \end{cases} \tag{7}$$

defines a step function of unity height. The refractive indexes in the core, n_c, and in the regions adjacent to the core, n_x and n_y, are related to those of our UV-written channel waveguides as

$$n_c = n_{\rm UV} = n_f + \Delta n_{\rm UV}, \quad n_x = n_s, \quad n_y = n_f. \tag{8}$$

The model differs from the exact profile by the depression of the refractive-index

$$n_d = \left(n_x^2 + n_y^2 - n_c^2\right)^{1/2} < n_x, n_y \tag{9}$$

in the corner regions $|x| > a_x, |y| > a_y$, marked by the shading in Fig. 7(b).

Neglecting the influence of the field in the corner regions, Marcatili solved the problem by decomposing the waveguide structure into two planar waveguides [14], one with the profile along the x direction

$$n_x^2(x) = \begin{cases} n_x^2 & \text{for } |x| < a_x \\ n_d^2 & \text{for } |x| > a_x \end{cases} \tag{10}$$

and the other with the profile along the y direction

$$n_y^2(y) = \begin{cases} n_y^2 & \text{for } |y| < a_y \\ n_d^2 & \text{for } |y| > a_y \end{cases} \tag{11}$$

according to Fig. 7(b).

Once the propagation constants β_x and β_y for the two planar waveguides with index profiles $n_x^2(x)$ and $n_y^2(y)$, respectively, have been found, the propagation constant β of the composite rectangular channel waveguide is given by [14]

$$\beta^2 = \beta_x^2 + \beta_y^2 - k^2 n_d^2 \tag{12}$$

where $k = 2\pi/\lambda$ is the wave number as defined in Section III. The propagation constants β_x and β_y of the two constituting planar waveguides are obtained from the well-known eigenvalue equations [16] for the fundamental TE mode

$$W_t = U_t \tan U_t, \quad t = x, y \tag{13}$$

and for the fundamental TM mode

$$W_t = (1 - 2\Delta_t) U_t \tan U_t, \quad t = x, y. \tag{14}$$

Here

$$\begin{aligned} U_t &= a_t \sqrt{k^2 n_t^2 - \beta_t^2}, \\ W_t &= a_t \sqrt{\beta_t^2 - k^2 n_d^2}, \quad t = x, y \end{aligned} \tag{15}$$

are the usual modal parameters [16], and

$$\Delta_t = \frac{n_t^2 - n_d^2}{2n_t^2} \simeq \frac{n_t - n_d}{n_t}, \quad t = x, y \tag{16}$$

are relative refractive-index differences. More explicitly, we have

$$\Delta_x = \frac{n_c^2 - n_y^2}{2n_x^2} \simeq \frac{n_c - n_y}{n_x} \simeq \frac{n_c - n_y}{n_c} \tag{17}$$

$$\Delta_y = \frac{n_c^2 - n_x^2}{2n_y^2} \simeq \frac{n_c - n_x}{n_y} \simeq \frac{n_c - n_x}{n_c}. \tag{18}$$

For the small refractive-index differences considered here, any of the known refractive indexes n_c, n_x, or n_y can be inserted in the denominator, as this would only introduce a very small error of second order in the refractive-index differences. Note that n_y appears in Δ_x, and n_x appears in Δ_y.

For our UV-written waveguides we have

$$\Delta_x = \frac{n_{\rm UV}^2 - n_f^2}{2n_s^2} \simeq \frac{n_{\rm UV} - n_f}{n_s} = \frac{\Delta n_{\rm UV}}{n_s} \tag{19}$$

$$\Delta_y = \frac{n_{\rm UV}^2 - n_s^2}{2n_f^2} \simeq \frac{n_{\rm UV} - n_s}{n_f} \simeq \frac{\Delta n_{\rm UV} + n_f - n_s}{n_s}. \tag{20}$$

The approximations are valid for the small index differences of the waveguides considered here.

The solutions of the modal eigenvalue equations (13) and (14) depend only on the values of the normalized frequencies

$$\begin{aligned} V_t &= k a_t \sqrt{n_t^2 - n_d^2} \\ &= \sqrt{U_t^2 + W_t^2}, \quad t = x, y \end{aligned} \tag{21}$$

and, in case of the TM modes, on the relative refractive-index differences Δ_t. More explicitly

$$V_x = ka_x\sqrt{n_c^2 - n_y^2}, \quad V_y = ka_y\sqrt{n_c^2 - n_x^2}. \tag{22}$$

Here, n_y appears in V_x, and n_x appears in V_y. For the UV-written waveguides we have

$$V_x = ka_x\sqrt{n_{\mathrm{UV}}^2 - n_f^2}, \quad V_y = ka_y\sqrt{n_{\mathrm{UV}}^2 - n_s^2}. \tag{23}$$

In order to obtain the form birefringence of the UV-written channel waveguide accurately to first order in Δ_x and Δ_y [15], we could proceed by searching for the propagation constants of the two orthogonally polarized fundamental modes of the composite structure according to (12) and afterwards subtracting them from each other. However, we may simplify the problem as follows.

The birefringence is defined as [see (1)]

$$\begin{aligned}\delta n^{\mathrm{eff}} &= \frac{\delta\beta}{k} = \frac{\beta_{\mathrm{TE}} - \beta_{\mathrm{TM}}}{k} \\ &\simeq \frac{1}{2kn_c}\left(\beta_{\mathrm{TE}}^2 - \beta_{\mathrm{TM}}^2\right)\end{aligned} \tag{24}$$

With the definitions below (1) [see Fig. 7] the TE-mode problem of the composite structure requires to find the propagation constant $\beta_{x\,\mathrm{TM}}$ of the TM mode of the planar waveguide varying as $n_x^2(x)$ along the x direction and the propagation constant $\beta_{y\,\mathrm{TE}}$ of the TE mode of the planar waveguide with profile $n_y^2(y)$ along the y direction. Analogously, the TM-mode problem of the composite structure requires to find the propagation constant $\beta_{x\,\mathrm{TE}}$ of the TE mode of the planar waveguide varying as $n_x^2(x)$ along the x direction and the propagation constant $\beta_{y\,\mathrm{TM}}$ of the TM mode of the planar waveguide with profile $n_y^2(y)$ along the y direction. The propagation constants of the TE and TM modes of the composite channel waveguide structure are then obtained as

$$\beta_{\mathrm{TE}}^2 = \beta_{x\,\mathrm{TM}}^2 + \beta_{y\,\mathrm{TE}}^2 - k^2n_d^2 \tag{25}$$

and

$$\beta_{\mathrm{TM}}^2 = \beta_{x\,\mathrm{TE}}^2 + \beta_{y\,\mathrm{TM}}^2 - k^2n_d^2 \tag{26}$$

respectively. Inserting into (24) yields

$$\delta n^{\mathrm{eff}} = \frac{1}{2k^2n_c}\left[\left(\beta_{y\,\mathrm{TE}}^2 - \beta_{y\,\mathrm{TM}}^2\right) - \left(\beta_{x\,\mathrm{TE}}^2 - \beta_{x\,\mathrm{TM}}^2\right)\right] \tag{27}$$

$$\simeq \frac{1}{k}\left[\left(\beta_{y\,\mathrm{TE}} - \beta_{y\,\mathrm{TM}}\right) - \left(\beta_{x\,\mathrm{TE}} - \beta_{x\,\mathrm{TM}}\right)\right] \tag{28}$$

$$= \frac{\delta\beta_y - \delta\beta_x}{k} = \delta n_y^{\mathrm{eff}} - \delta n_x^{\mathrm{eff}}. \tag{29}$$

We see that the birefringence δn^{eff} of the composite weakly guiding waveguide structure simply equals the difference of the birefringence values

$$\delta n_y^{\mathrm{eff}} = \frac{\beta_{y\,\mathrm{TE}} - \beta_{y\,\mathrm{TM}}}{k} \tag{30}$$

and

$$\delta n_x^{\mathrm{eff}} = \frac{\beta_{x\,\mathrm{TE}} - \beta_{x\,\mathrm{TM}}}{k} \tag{31}$$

of the two constituting planar waveguides described by (11) and (10), respectively. This may greatly simplify the analysis if the results of planar waveguides are used. In particular, for the present small index differences, linearization of the eigenvalue equation (14) in Δ_t relates the eigenvalue U_{TM} of the TM mode on a planar waveguide to the eigenvalue U_{TE} of the corresponding TE mode of the same mode number as

$$U_{\mathrm{TM}} \simeq U_{\mathrm{TE}} + \frac{2U_{\mathrm{TE}}W_{\mathrm{TE}}^2}{V^2(1 + W_{\mathrm{TE}})}\Delta \tag{32}$$

where $V = \sqrt{U_{\mathrm{TE}}^2 + W_{\mathrm{TE}}^2}$ is the normalized frequency of the corresponding planar waveguide according to (22). With (15) we find a simple expression for the form birefringence

$$\delta n^{\mathrm{eff}} = n_c\left[\Delta_y^2\frac{4U_y^2W_y^2}{V_y^4(1 + W_y)} - \Delta_x^2\frac{4U_x^2W_x^2}{V_x^4(1 + W_x)}\right]. \tag{33}$$

The modal parameters U_t and W_t have to be calculated only for the TE modes of the waveguides with the profile variation along $x(t = x)$ or $y(t = y)$.

With Garmire's approximation [17] for the fundamental TE-mode eigenvalue

$$U_{\mathrm{TE}} \simeq \frac{\sqrt{1 + 2V^2} - 1}{V} \tag{34}$$

we may approximate the normalized form birefringence of a weakly guiding planar waveguide

$$B_F(V) = \frac{\beta_{\mathrm{TE}} - \beta_{\mathrm{TM}}}{kn_c\Delta^2} = \frac{4U_{\mathrm{TE}}^2W_{\mathrm{TE}}^2}{V^4(1 + W_{\mathrm{TE}})} \tag{35}$$

by a formula, which is explicit in the given normalized frequency V, as

$$B_F(V) \simeq \frac{4}{V^7}\frac{(\sqrt{1 + 2V^2} - 1)^2[V^4 - (\sqrt{1 + 2V^2} - 1)^2]}{V + [V^4 - (\sqrt{1 + 2V^2} - 1)^2]^{1/2}}. \tag{36}$$

Fig. 8 shows the normalized form birefringence $B_F(V)$ as calculated from the exact formula (35) by a solid line and from the explicit approximation (36) by a dashed line. The agreement is sufficiently good for most practical applications.

From (33) to (36), we obtain an explicit formula for the form birefringence of the general weakly guiding rectangular channel waveguides of Fig. 7 as

$$\delta n^{\mathrm{eff}} = n_c\left[\Delta_y^2B_F(V_y) - \Delta_x^2B_F(V_x)\right] \tag{37}$$

for which no numerical iterations are necessary. According to Fig. 7, the required quantities Δ_t and V_t with $t = x, y$ follow from (17), (18), and (22). For our UV-written channel waveguides these quantities are obtained from (8). Due to the small refractive-index differences, any of the almost equal refractive indexes n_c, n_x, or n_y can be inserted in front of the square brackets in (37).

Fig. 9 shows the form birefringence calculated from (37) and (36) for our UV-written waveguides for various channel half widths a_x versus the UV-induced refractive-index contribution Δn_{UV}. The unexposed ($\Delta n_{\mathrm{UV}} = 0$) planar waveguide

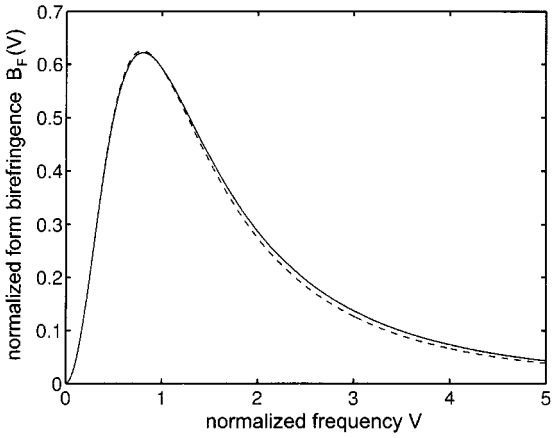

Fig. 8. Normalized form birefringence $B_F(V)$ of weakly guiding planar step-index waveguides. The solid line shows exact values from (35), and the dashed line was calculated from the approximation formula (36).

sample type A in Fig. 9(a) has a smaller form birefringence than sample type B in Fig. 9(b). This comes clearly from the different thicknesses $2a_y$ of the two planar waveguides. Since type A has a larger thickness than type B, the field in waveguide type A is more strongly confined to the core and the intensity at the index step of the film/substrate interface $|y| = a_y$, which causes the birefringence, is weaker. The difference can directly be read from Fig. 8 with $V_y = 2.06$ for type A and $V_y = 1.20$ for type B. The UV writing $(\Delta n_{\mathrm{UV}} > 0)$ increases the refractive-index difference which leads to an increase of the form birefringence. For broad UV-written cores, e.g., $a_x = 10$ μm, the channel waveguides behave very similarly like planar waveguides and the birefringence increases monotonously with Δn_{UV}. The asymptotic behavior for growing $\Delta_y \cong (n_f - n_c + \Delta n_{\mathrm{UV}})/n_c$ and thus for $V_y \gg 1$, while $\Delta_y \ll 1$, follows from [16] $U(V \gg 1) = \pi/2$ for the planar waveguide and from $B_F(V \gg 1) = \pi^2/V^3$ as $\delta n_y^{\mathrm{eff}} = \pi^2\sqrt{2\Delta_y}/4k^3a_y^3n_c^2$, and the slope of $\delta n_y^{\mathrm{eff}}$ versus Δn_{UV} decreases while remaining positive according to the asymptotic square-root function $\sqrt{2\Delta_y}$. For smaller core widths, e.g. $a_x = 1$ μm, the planar character gets lost as the field becomes also confined along the x coordinate. Effectively, the field becomes nearly circularly symmetric and the form birefringence is cancelled to zero similarly like in round optical fibers. For waveguide A, this happens for $a_x = 1$ μm and $\Delta n_{\mathrm{UV}} = 9.2 \times 10^{-3}$, as well as for $a_x = 2$ μm and $\Delta n_{\mathrm{UV}} = 1.18 \times 10^{-2}$. For even larger values of Δn_{UV}, the form birefringence of these waveguides increases again with opposite sign.

Practical UV-written refractive-index profiles are nonsymmetric due to the attenuation of the writing UV-laser beam. This asymmetry can be taken into account by calculating the birefringence by the effective-index method [18] using the analytical eigenvalue equation for step-index waveguides with an exponential UV-written contribution to the refractive-index profile [19]. Experimental results for the birefringence in our UV-written channel waveguides and theoretical results for the form birefringence of this section have been compared in Section IV.

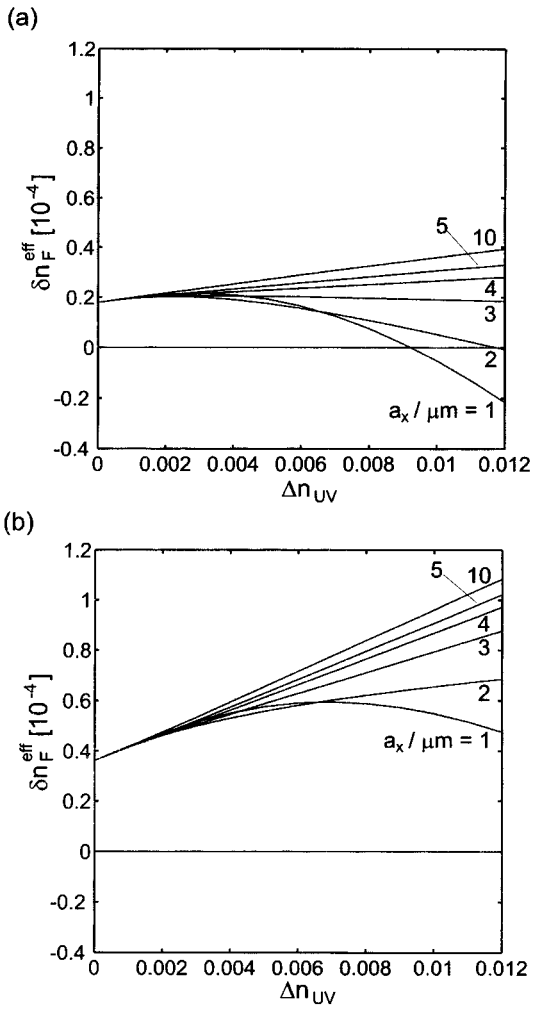

Fig. 9. Form birefringence δn^{eff} for (a) waveguides in sample type A with film thickness $2a_y = 6$ μm and for (b) waveguides in sample type B with film thickness $2a_y = 3.5$ μm as calculated by (37) and (36).

VI. Conclusion

In conclusion a technique for measuring the birefringence of integrated optical waveguides by using magneto-optical polarization-mode coupling has been presented. We have demonstrated this method for measuring the birefringence of UV-written channel waveguides in both silica-on-silicon and silica-on-silica. It has been shown for UV-written waveguides in silica-on-silicon that the waveguide birefringence is substantially reduced with increasing UV-writing power. It has been demonstrated further that for UV-written waveguides in silica-on-silica the waveguide birefringence is nearly independent of the UV-writing power. An analytical formula for the form birefringence of rectangular channel waveguides has been developed and the theoretical results have been compared with the measurements.

References

[1] G. E. Kohnke, C. H. Henry, E. J. Laskowski, M. A. Cappuzzo, T. A. Strasser, and A. E. White, "Silica based Mach-Zehnder add-drop filter fabricated with UV induced gratings," *Electron. Lett.*, vol. 32, pp. 1579–1580, 1996.

[2] C. K. Madsen, T. A. Strasser, M. A. Milbrodt, C. H. Henry, A. J. Bruce, and J. J. DeMarco, "Planar waveguide add/drop filter employing a mode-converting grating in an adiabatic coupler," in *Integr. Photon. Res. Conf.*, Victoria, BC, Canada, Mar. 29–Apr. 3 1998, pp. 102–104. IMG5.
[3] J. Hübner, J. M. Jouanno, J. E. Pedersen, R. Kromann, T. Feuchter, and M. Kristensen, "Strong Bragg gratings in non sensitized low loss planar waveguides as building blocks for WDM network components," *Proc. SPIE*, vol. 2998, pp. 100–110, 1997.
[4] D. Johlen, P. Klose, and E. Brinkmeyer, "UV-written directional couplers in silica-on-silicon," in *Tech. Dig. Optic. Fiber Commun. Conf.*, vol. 6, Washington, DC, 1997, Optic. Soc. Amer., Paper ThI5, pp. 279–280.
[5] C. V. Poulsen, J. Hübner, T. Rasmussen, L.-U. A. Andersen, and M. Kristensen, "Characterization of dispersion properties in planar waveguides using UV-induced Bragg gratings," *Electron. Lett.*, vol. 31, pp. 1437–1438, 1995.
[6] J. Albert, F. Bilodeau, D. C. Johnson, K. O. Hill, S. J. Mihailov, D. Stryckman, T. Kitagawa, and Y. Hibino, "Polarization-independent strong Bragg gratings in planar lightwave circuits," *Electron. Lett.*, vol. 34, pp. 485–486, 1998.
[7] R. Stolte and R. Ulrich, "Electro-optic and thermo-optic measurements of birefringence of $LiNbO_3$ waveguides," *Opt. Lett.*, vol. 20, pp. 142–144, 1995.
[8] R. Eckhardt and R. Ulrich, "Mode-beating spectroscopy in a few-mode optical guide," *Appl. Phys. Lett.*, vol. 63, pp. 284–286, 1993.
[9] R. Stolte and R. Ulrich, "High resolution spatial interferometry of guided optical waves," *Electron. Lett.*, vol. 32, pp. 814–816, 1996.
[10] S. C. Rashleigh, "Wavelength dependence of birefringence in highly birefringent fibers," *Opt. Lett.*, vol. 76, pp. 294–296, 1982.
[11] T. A. Strasser, T. Erdogan, A. E. White, V. Mizrahi, and P. Lemaire, "Ultraviolet laser fabrication of strong, nearly polarization-independent Bragg reflectors in germanium-doped silica waveguides on silica substrates," *Appl. Phys. Lett.*, vol. 65, pp. 3308–3310, 1994.
[12] D. Johlen, P. Klose, A. Ewald, and E. Brinkmeyer, "Non-reflecting narrow-band fiber optical Fabry-Perot transmission filter," in *Bragg Gratings, Photosensitivity and Poling in Glass Fibers and Waveguides: Applications and Fundamentals Meeting*, 1997, OSA paper BSuC5, pp. 42–44.
[13] T. Erdogan and V. Mizrahi, "Characterization of UV-induced birefringence in photosensitive Ge-doped silica optical fibers," *J. Opt. Soc. Amer. B*, vol. 11, pp. 2100–2105, 1994.
[14] E. A. J. Marcatili, "Dielectric rectangular waveguide and directional coupler for integrated optics," *Bell Syst. Tech. J.*, vol. 48, pp. 2071–2102, 1969.
[15] H. Renner, "Polarization characteristics of optical waveguides with separable symmetric refractive-index profiles," *J. Opt. Soc. Amer. A*, vol. 15, pp. 1401–1410, 1998.
[16] A. W. Snyder and J. D. Love, *Optical Waveguide Theory*. London, U.K.: Chapman and Hall, 1983.
[17] E. Garmire, "Simple solutions for modeling symmetric step-index dielectric waveguides," *J. Lightwave Technol.*, vol. 6, pp. 1105–1108, 1988.
[18] M. J. Adams, *An Introduction to Optical Waveguides*. New York: Wiley, 1981.
[19] H. Renner, "Modes of UV-written planar waveguides," *Opt. Lett.*, vol. 23, pp. 111–113, 1998.

Dietmar Johlen, photograph and biography not available at the time of publication.

Gunnar Stolze, photograph and biography not available at the time of publication.

Hagen Renner, photograph and biography not available at the time of publication.

Ernst Brinkmeyer, photograph and biography not available at the time of publication.